Synthesis, structural, spectroscopic and thermoanalytical study of sol-gel derived SiO_2-CaO-P_2O_5 gel and ceramic materials

Michelina Catauro[a,*] Alessandro Dell'Era[b], Stefano Vecchio Ciprioti[c,*]

[a]Department of Industrial and Information Engineering, Second University of Naples, via Roma 29, Aversa (CE), Italy
[b]Department D.M.E., 'Guglielmo Marconi' University, via Plinio 44, Roma, Italy
[c]Department S.B.A.I., Sapienza University of Rome, via del Castro Laurenziano 7, Roma, Italy

Abstract

In the present work bioactive powders of the ternary $SiO_2 \cdot CaO \cdot P_2O_5$ systems, which differ in the Ca/P molar ratio, were synthesized by means of a sol–gel route, using tetraethyl orthosilicate (TEOS, $Si(OC_2H_5)_4$), calcium nitrate tetrahydrate ($Ca(NO_3)_2 \cdot 4H_2O$) and triethyl phosphate (TEP, $OP(OC_2H_5)_3$) as precursors of SiO_2, CaO and P_2O_5, respectively. In order to investigate the influence of the relative amount of each phase (in this study: SiO_2, CaO and P_2O_5) the thermal properties of the synthesized gel-glass materials were studied as a function of the Ca/P molar ratio using thermogravimetric and differential thermal analysis (TG/DTA). After dehydration (in a single step), described from a kinetic point of view as a simple water evaporation without rupture of chemical bonds, all gels undergo a complex multi-step decomposition with endo and exothermic effects, followed by crystallization of calcium silicate phases at about 950°C. Furthermore, Fourier Transform Infrared Spectroscopy (FTIR), X-ray diffraction (XRD) and Scanning Electron Microscopy, coupled with energy dispersive spectroscopy (SEM/EDS), allowed us to detect the chemical modifications induced by modifying the Ca/P molar ratio and the sintering. This process is obtained by thermal treatment of the gel-glass precursors after analyzing their thermal behavior in the temperature range 600–1000 °C, with the aim to convert them into ceramic powders, suitable for their applications. The results revealed that when temperature is up to 900 °C, crystallization occurs and pseudowollastonite and wollastonite were formed. Finally, the amount of pseudowollastonite decreased with increasing the sintering temperature, while that of wollastonite increased.

Keywords: Sol–gel method, SiO_2 –CaO–P_2O_5, TG/DTA, FTIR, XRD, SEM/EDS, crystallization, pseudowollastonite, wollastonite.

* Corresponding Authors:
(M. Catauro) E-mail Address: michelina.catauro@unina2.it for the synthesis and characterization of materials
(S. Vecchio Ciprioti) E-mail Address: stefano.vecchio@uniroma1.it for thermal behavior and kinetics

1. Introduction

The need for durable and high-performances medical devices has induced researchers in the biomedical field to develop several classes of materials with high biocompatibility. Another important requirement of a material potentially useful in the dental and orthopaedic field is bioactivity, which is the ability to bond living bones [1]. In the last years, several classes of materials such as metals, alloys, polymers, glass/ceramics and composites materials have been proposed for this application [2, 3]. Among them, glasses and ceramics have caught the attention of many research groups. The first bioglass (45S5) was discovered in 1971 by L. Hench at al. [4]. Its composition was 46.1 mol% SiO_2, 26.9 mol% CaO, 24.4 mol% Na_2O and 2.5 mol%P_2O_5. Since then, many compositions were explored [5, 6], which differ in the type of oxide added as well as in the composition (molar percentages) considered. In particular, ternary systems $SiO_2 \cdot CaO \cdot P_2O_5$ with low P_2O_5 content have shown to constitute a promising class of bioactive materials for bone repair and substitution [7-11]. In addition to composition, the preparation method can also influence the biological properties of the bioactive glasses and ceramics. It is proved [12, 13] that glasses and ceramic synthesized by the sol-gel methods are more bioactive than those ones obtained by the melt-quench technique. The sol-gel is a method that allows obtaining glassy materials using a low-temperature hydrolysis and condensation process. It starts when water is added to a solution of metal alkoxide in ethanol and stops when the formation of an inorganic and rigid network (the gel) is formed. With further drying and heat treatment, the obtained gel can be converted into dense ceramic or glass. The chemical nature of precursors and the low temperature ensure good homogenization of the reactants, uniformity of the obtained gels and prevent potential crystallization and phase separation. Moreover, the formation of a large number of residual hydroxyl groups occurs as a result of the chemical sol-gel reactions and some of them remain even after the thermal stabilization of the materials. Such –OH groups can stimulate the hydroxyapatite nucleation on the material surface both during *in vitro* tests and *in vivo*, promoting the material easier osseointegration and, thus, making the sol-gel glasses and ceramics generally very bioactive.

Moreover, sol-gel $SiO_2 \cdot CaO$ and $SiO_2 \cdot CaO \cdot P_2O_5$ materials are also very biocompatible. The sol–gel glasses, in fact, are generally mesoporous and, thus, have a larger surface area than melt-derived glasses of similar composition. This feature allows a potentially more rapid degradation rates of the sol-gel derived $SiO_2 \cdot CaO$ and $SiO_2 \cdot CaO \cdot P_2O_5$ glasses and their dissolution and degradation products can promote the bone tissue growth. Soluble silica and calcium ions, in fact, are able to induce osteogenesis by activation and stimulation of osteoprogenitor cells at the implant site [14, 15].

The biological properties of the sol-gel materials are also affected by the heat treatment used in order to stabilize and densify the materials, because the heating may induce structural modifications. In a previous work [11], the authors proved that $SiO_2 \cdot CaO \cdot P_2O_5$ sol-gel glasses are bioactive and biocompatible and the samples containing high calcium content, calcined at 600°C, can improve their biological performance. Therefore, in order to develop rationally $SiO_2 \cdot CaO \cdot P_2O_5$ gels and glasses/ceramic to be used as bioactive and biocompatible materials, it is necessary a full comprehension of their thermal behaviour by means of thermal analysis and investigation of the processes occurring during heating from a kinetic point of view.

In the present work, the thermal behaviour of $SiO_2 \cdot CaO \cdot P_2O_5$ materials synthesized by sol-gel method was studied by simultaneous thermogravimetry and differential thermal analysis (TG/DTA) and the chemical, spectroscopic and structural characterization of the synthesized materials was carried out as a function of both the molar Ca/P ratio and the heat-treatment used by FTIR, XRD and SEM analysis.

2. Materials and methods

2.1. Sol–gel synthesis

Sol-gel glasses were synthesized starting from tetraethyl orthosilicate (TEOS, $Si(OC_2H_5)_4$, Sigma Aldrich), calcium nitrate tetrahydrate ($Ca(NO_3)_2 \cdot 4H_2O$, Sigma Aldrich) and triethyl phosphate

(TEP, $C_6H_{15}O_4P$, Sigma Aldrich) as sources of SiO_2, CaO and P_2O_5 respectively. TEOS was added under stirring to a solution of nitric acid ($HNO_3 \geq 65\%$, Sigma-Aldrich), water and ethanol (EtOH, 99,8% Sigma-Aldrich). After 30 min, TEP was added to the obtained solution. After 30 min under stirring, calcium nitrate tetrahydrate was dissolved slowly and the sol was stirred for 3h at room temperature. The final mixture appears homogenous and transparent and the molar ratio of TEOS/H_2O was 1:4, H_2O/EtOH was 1:1 and the molar ratio of HNO_3 /(TEOS+TEP) was 1:16.

Four formulations of samples, which differ for the molar ratio Ca/P, were synthesized according to the procedure reported in the previous paragraph and their chemical composition is reported in Table 1. The samples were left to gel at room temperature. The obtained gels appear transparent, homogeneous and colorless (Fig. 1). Subsequently, they were treated at 120°C, 600°C and 1000°C for 3h. The heating was carried out in a furnace and the temperature increase to 9 °C/min. The flow chart of the process is shown in Fig. 2.

Table 1 Chemical composition of the synthesized glasses

Label	Ca/P molar ratio	Composition		
		CaO/%$_{mol}$	SiO_2/%$_{mol}$	P_2O_5/%$_{mol}$
63S32C5P	3	63	32	5
62S35C3P	6	62	35	3
61S37C2P	9	61	37	2
61S38C1P	19	61	38	1

2.2. Chemical and spectroscopic characterization

The chemical and the structural characterization of the obtained glasses were carried out on the all the prepared samples after each heat treatment, in order to follow the evolution of the system as a function of both the temperature and the Ca/P molar ratio.

Synthesized glasses were analyzed using Fourier transform infrared spectroscopy (FTIR) to characterize their chemical structure. Prestige 21 spectrophotometer (Shimadzu, Tokyo, Japan) was used for record transmittance spectra in the 400-4000 cm^{-1} region with a resolution of 2 cm^{-1} (45 scans), the instrument was equipped with DTGS KBr (Deuterated Tryglycine Sulphate with

potassium bromide windows) detector. KBr pelletised disks containing 2 mg of sample and 200 mg KBr were made. FTIR spectra were analyzed by Prestige software (IRsolution).

2.3. Thermal analysis measurements

The thermal behavior of the gels was investigated by using a Stanton Redcroft STA-1500 simultaneous TG/DTA apparatus, consisting of two Pt crucibles of cylindrical shape (with Pt–Pt/Rh thermocouples): the reference crucible was covered with about 20–25 mg of alumina, while that of the sample (whose size was approximately of 20–25 mg), was first filled with the minimum amount to uniformly cover its bottom surface area to avoid any possible reaction between the sample and Pt a high temperature. TG/DTA experiments were carried out under inert Ar atmosphere (50 ml min^{-1}) at a constant heating rate of 10 K min^{-1} from room temperature to 1200 °C. TG experiments were carried out at heating rates of 5, 7, 10 and 15 °C min^{-1} (under the same gas atmosphere used for thermal behavior study) and TG data related to mass losses recorded during the occurrence of dehydration were exported in ASCII format before being processed to perform the dehydration kinetic analysis. Calibration of sample temperature was performed using very pure indium and zinc reference materials and a final average uncertainty of ±0.5K was estimated over the whole temperature range.

2.4. SEM-EDX and XRD measurements

Scanning electron microscopy with energy dispersive X-ray spectroscopy (SEM-EDX, Quanta 200, FEI, the Netherlands) was used to investigate the morphologies of sol-gel glasses. Samples were fixed on aluminum stubs with colloidal graphite and metalized with gold (K550X Sputter Coater, Emitech, East Sussex, UK). X-ray diffraction (XRD) experiments were performed on a PHILIPS diffractometer equipped with a PW1830 generator, tungsten lamp and Cu anode. Cu-Kα radiation (λ=0.15418 nm) was employed.

3. Results and Discussion

3.1. Thermal behavior and kinetic analysis of dehydration

In order to make a correct interpretation of the thermal behavior and of the FT-IR spectra, in addition to the samples object of this study (having molar ratios Ca/P = 3, 6, 9 and 19), the starting material consisting of a gel glass containing CaO and SiO_2 in molar percentages of 70 and 30%, respectively (denoted thereafter as 70C30C), was synthesized and used as control.

The TG/DTA curves of all the material investigated are shown in Fig. 3. All material investigated undergo a three-step processes, the first of which is due to a simple dehydration (characterized by a single step of mass loss of about 22-27% accompanied by a single endothermic event, recorded between room temperature and 130°C by the TG and DTA curves, respectively). Actually, the experimental conditions used (Ar flowing atmosphere and 10 K min^{-1}) avoid the possibility to discriminate the release water molecules physically bounded that are lost at lower temperature (<100°C) from the crystallization water, chemically bounded to Si-O-Si bridges, that evolved at higher temperatures. Negligible differences were observed among the TG/DTA of the tested materials: the curves are practically superimposable. Only slightly higher amount of water is released by the sample 62S35C3P. Since this process can be approximately considered a single step, it was possible to apply a kinetic procedure to analyze it with the aim to verify if, in spite of the very similar thermal behavior of all the materials, some differences in the kinetics of water release can be evidenced. The integral isoconversional kinetic method of Ozawa-Flynn-Wall [16, 17], with the Doyle approximation [18], was considered, whose details were extensively reported in recently published papers [19-23]. The isoconversional E_α *vs.* α plot for dehydration is shown in Fig. 4*a-e*. A slight decreasing trend is observed for the E_α *vs.* α curves related to dehydration of all the materials, with values ranging from about 46 to 34 kJ mol^{-1}, thus suggesting that a reversible mechanism takes place [24]. This negligible variation of activation energy (within the estimated

uncertainties, always lower than ±8 kJ mol^{-1}) makes it possible the application of this method, according to the restrictions pointed out by Simon [25]. In addition, these values are in close agreement with the standard molar vaporization enthalpy of water (≈44 kJ mol^{-1}) and with those reported in literature for water evaporation from bulk or from clays [26]. These results can be reasonably explained by hypothesizing that no appreciable chemical bond dissociates during the water release that could theoretically increased the energy barrier represented by the activation energy. The second step takes place between 150 and 600°C (Fig. 3) and is made by two or three consecutive reactions with corresponding total mass losses of about 27-30%, the first of which seems to be correlated to the amount of P_2O_5 in the material: the higher is the P_2O_5 content, the higher is the mass loss. Several endothermic effects (two or three depending on the material) seem to be observed in this temperature range, and probably a slight exothermic one around 300°C that could be attributed to a possible decomposition of nitrates, used in the preparation of the sol precursors of this study as well as to other undesired components of the starting material. As stressed in a recent study, coherently to the findings of Martin and co-workers [13], a not negligible amount of calcium nitrate (soluble in the sol) could still remain in solution during the occurrence of the condensation process and once water and solvent were driven off it coats the silica network [13, 19]. Finally, an exothermic effect without appreciable mass losses, clearly observed in the DTA curve of 70S30C around 950°C and with negligible intensity for the samples containing P_2O_5, is ascribed to crystallization of calcium silicates, similarly to what has been already observed for other similar materials [19, 27-29].

3.2. Spectroscopic characterization

Fig. 5 shows the spectra of the synthesized $SiO_2 \cdot CaO \cdot P_2O_5$ samples heat-treated at 120°C (Fig. 5a) compared with those ones of pure $Ca(NO_3)_2 \cdot 4H_2O$, and the control materials: $CaO \cdot SiO_2$, $P_2O_5 \cdot SiO_2$, and SiO_2 (Fig. 5b). The spectra of the $SiO_2 \cdot CaO \cdot P_2O_5$ samples are very similar to that of

184 pure $Ca(NO_3)_2 \cdot 4H_2O$. All typical peaks of the salt are found, like the strong bands at 1423 and 1354
185 cm^{-1}, the sharp ones at 1382, 1047, 823 cm^{-1} and the weak at 738 cm^{-1}, due to asymmetric and
186 symmetric stretching vibrations and bending modes of nitrate ions [30]. Moreover, in the spectra of
187 the samples with high amount of P_2O_5 (63S32C5P and 62S35C3P) some bands are visible which
188 are ascribable to vibration modes of SiO_2 and P_2O_5. In particular, the bands at 1165 and 1210 cm^{-1},
189 observed even in $SiO_2 \cdot P_2O_5$ spectrum and absent in $SiO_2 \cdot CaO$ spectrum (Fig. 5b), are due to the
190 asymmetric stretching vibrations of the P-O groups in Q^2 and Q^1 structural units, respectively [31].
191 The bands at 1082 and 958 cm^{-1} prove that the formation of the silica network occurred. Those
192 bands are assigned to the symmetric stretching of SiO_4 tetrahedra [32] and the surface silanol
193 groups [33] respectively. The intensity of the Si-O stretching band at 1082 cm^{-1} decreases with the
194 increase of the calcium nitrate amount and appears very weak in the spectrum of 61S38C1P sample.
195 To prove that the band at 1082 cm^{-1} is present in the FTIR spectra of all the samples, an enlarged
196 view of the spectral region between 1300 and 800 cm^{-1} is shown in Fig. 6. This band at 958 cm^{-1} is
197 found at 937 cm^{-1} in the spectrum of pure SiO_2 (Fig. 5b). The up-shift is probably due to the
198 interaction of the Si-OH groups with the ionic species present in the obtained materials (Ca^{2+}, PO_4^{3-},
199 PO_3^-, $P_2O_7^{4-}$, etc.).
200 Fig. 7 shows the FTIR spectra of the synthesized $SiO_2 \cdot CaO \cdot P_2O_5$ samples compared with pure SiO_2
201 spectrum after heat treatment at 600°C. The displacement of all nitrate signals is evident. It is
202 known that calcium is not incorporated into the silicate network until heat-treating beyond 350°C.
203 During the condensation reaction, which occurs in the sol, calcium nitrate remains in solution as
204 silica nanoparticles are formed and coalesce. During drying, the condensation by-products are
205 driven off and calcium nitrate coats the silica network [13]. This phenomenon explains why the
206 sample spectra recorded after treatment at 120°C are similar to that of pure $Ca(NO_3)_2 \cdot 4H_2O$.
207 However, as the temperature exceeds 400°C, calcium ions enter the network by diffusion and the
208 nitrate by-products (mainly gaseous NO_2 and O_2 produced by thermal degradation of the nitrate
209 ions) are driven off at temperature higher than 550°C [13]. The displacement of all nitrate bands

allows even the appearance of a strong signal due to the asymmetric stretching mode of Si-O-Si bonds. This band is recorded at 1090 cm^{-1} in the spectrum of pure SiO_2, whereas it appears shifted to 1078 cm^{-1} with a shoulder at 1050 cm^{-1} in the spectrum of 63S32C5P. When the calcium content increases the shoulder becomes a distinct band at 1050 cm^{-1}. Moreover, with the increase of the CaO amount, the strong band shifted toward lower wavenumber: the peak is seen at 1090 cm^{-1} in the spectrum of pure SiO_2, while it appears as a shoulder at 1050 cm^{-1} in the spectra of the gel-glasses with high CaO content. The shift toward lower wavenumber and the broadening of the Si-O-Si band are caused by the presence of CaO modified oxide, which is able to increase the number of non-bridging oxygen atoms [34, 35]. The high Ca^{2+} content causes also the appearance of a band at 1452 cm^{-1} in the spectra of both the 61S37C2P and 61S38C1P samples. This band can be ascribed to the presence of $CaCO_3$, due to Ca^{2+}, not incorporated in the network, carbonated by atmospheric CO_2 [36].

Some changes involve also the phosphorous species. The bands at 1165 and 1210 cm^{-1} disappear after heat-treatment at 600°C and two weak peaks at 572 and 603 cm^{-1} appear which are assigned to the P–O bending vibration corresponding to the crystalline phosphates. The displacement of the signal related to the presence of P-O groups in Q^2 and Q^1 structural units suggests that the small clusters of P-species dispersed in the silicate matrix broke and a larger amount of Q^0 structural units (PO_4^{3-}) forms. Moreover, in the spectrum of the sample with high P content (63S32C5P), another shoulder at 960 cm^{-1} is seen, due to P-O vibration [37, 38]. Fig. 8 shows the FTIR spectra of synthesized $SiO_2 \cdot CaO \cdot P_2O_5$ samples after heat treatment at 1000°C. An enlarged view of the changed region is reported with the aim to observe better these peaks. The spectra show all the typical peaks of wollastonite ($CaSiO_3$) (1070, 1030, 950, 900 and 800 cm^{-1}) and pseudowollastonite [$Ca_3(Si_3O_9)$, 710 cm^{-1}]. Moreover, the two bands at 605 and 570 cm^{-1} confirm the presence of tricalcium phosphate (TCP) and calcium phosphate silicate [$Ca_{15}(PO_4)_2(SiO_4)_6$] [23].

3.3. Structural characterization by SEM-EDX and XRD measurements

Fig. 9 presents SEM micrographs of synthesized and thermally treated samples. In panel A and B can be observed 63S32C5P and 61S38C1P after 120°C respectively. The structure appears compact and inhomogeneity are not present below 1 μm. EDX analysis of the surface (inserted in panel A) confirms the composition of the materials. After the heat treatment at 600°C on the surface of the samples (Panel C and D) plate-like shaped structures appear with size of 3-5 μm. The heat treatment at 1200°C causes an increase of such plate-like crystals (Panel E and F). Their chemical composition Ca-reach, investigated by EDX analysis (Panel F), their characteristic morphology suggest that those structure are crystals, in accordance with Radev *et al.* [37]. The reported SEM images are in a good agreement with FT-IR and XRD analyses of the samples. X-ray diffraction pattern of fresh and calcined samples are reported in Fig. 10a-b, respectively. It is clearly evident that fresh samples are amorphous, while those calcined at 1200 °C revealed the formation of two crystalline calcium silicate phases: wollastonite and pseudowollastonite, thus confirming the findings of FTIR measurements.

By coupling the results of the study of their thermal behavior with the structural characterization it can be concluded that two temperatures should be considered for the thermal treatment of gel-glasses precursors. At 600°C water, nitrates, and all possible volatile decomposition products are eliminated, and a crystalline structure is going to appear (plate-like crystals), but is at 1200°C that crystallization of several calcium silicate phases takes place, showing a well-defined structural order, accompanied by an increase of crystal sizes.

4. Conclusions

In this manuscript we proposed the synthesis (by the sol-gel method) of four gel-glass materials based on the ternary SiO_2-CaO-P_2O_5 system with different compositions. A multi-technique approach (Fourier Transform Infrared Spectroscopy, X-ray diffraction, Scanning Electron Microscopy coupled with energy dispersive spectroscopy and simultaneous thermogravimetry and

differential thermal analysis (TG/DTA)) was considered to provide a complete characterization of the tested materials. The chemical and structural characterization proved that heating induces modification on the material. In particular, we focused our attention on thermal analysis techniques, which were found able to be a useful tool, in combination with the previously mentioned techniques, to analyze the thermal behavior of the materials investigated aiming at selecting the most suitable temperatures to thermally treat and transform them into ceramic ones, being the latter able to display a promising bioactivity.

References

[1] T. Kokubo, Bioactive glass ceramics: properties and applications, Biomaterials 12 (1991) 155-163.

[2] G. Manivasagam, D. Dhinasekaran, A. Rajamanickam, Biomedical implants: corrosion and its prevention - a review, Recent Pat. Corros. Sci. 2 (2010) 40-54.

[3] M. Catauro, F. Papale, F. Bollino, Characterization and biological properties of TiO_2/PCL hybrid layers prepared via sol-gel dip coating for surface modification of titanium implants, J. Non-Cryst. Solids 415 (2015) 9-15.

[4] L.L. Hench, R.J. Splinter, W.C. Allen, T.K. Greenlee, Bonding mechanism at interface of ceramic prosthetic materials, J. Biomed. Mater. Res 2 (1972) 117-141.

[5] L. Radev, V. Hristov, I. Michailova, M.H.V. Fernandes, I.M.M. Salvado, In vitro bioactivity of biphasic calcium phosphate silicate glass-ceramic in CaO- SiO_2- P_2O_5 system, Process. Appl. Ceram. 4 (2010) 15-24.

[6] M. Catauro, F. Papale, G. Roviello, C. Ferone, F. Bollino, M. Trifuoggi, C. Aurilio, Synthesis of SiO_2 and CaO rich calcium silicate systems via sol-gel process: Bioactivity, biocompatibility, and drug delivery tests, Journal of Biomedical Materials Research - Part A 102 (2014) 3087-3092.

[7] A. Balamurugan, G. Balossier, S. Kannan, J. Michel, A.H.S. Rebelo, J.M.F. Ferreira, Development and in vitro characterization of sol-gel derived CaO-P_2O_5-SiO_2-ZnO bioglass, Acta Biomater. 3 (2007) 255-262.

[8] D. Bizari, M. Rabiee, F. Moztarzadeh, M. Tahriri, S.H. Alavi, R. Masaeli, Synthesis, characterization and biological evaluation of sol-gel derived nanomaterial in the ternary system 64 % SiO_2 - 31 % CaO - 5 % P_2O_5 as a bioactive glass: in vitro study, Ceram.-Silik. 57 (2013) 201-209.

[9] P.I. Haris, P. Saravanapavan, J.R. Jones, S. Verrier, R. Beilby, V.J. Shirtliff, L.L. Hench, J.M. Polak, Binary CaO- SiO_2 gel-glasses for biomedical applications, Bio-Med. Mater. Eng. 14 (2004) 467-486.

[10] H.C. Li, D.G. Wang, J.H. Hu, C.Z. Chen, Influence of fluoride additions on biological and mechanical properties of Na_2O-CaO-SiO_2-P_2O_5 glass-ceramics, Mater. Sci. Eng. C 35 (2014) 171-178.

[11] M. Catauro, F. Bollino, R.A. Renella, F. Papale, Sol-gel synthesis of SiO_2-CaO-P_2O_5 glasses: Influence of the heat treatment on their bioactivity and biocompatibility, Ceram. Int. 41 (2015) 12578-12588.

[12] R. Gupta, A. Kumar, Bioactive materials for biomedical applications using sol-gel technology, Biomed. Mater. 3 (2008) 034005.

[13] R.A. Martin, S. Yue, J.V. Hanna, P.D. Lee, R.J. Newport, M.E. Smith, J.R. Jones, Characterizing the hierarchical structures of bioactive sol-gel silicate glass and hybrid scaffolds for bone regeneration, Philos. Trans. R. Soc. A 370 (2012) 1422-1443.

[14] S. Midha, T.B. Kim, W. Van Den Bergh, P.D. Lee, J.R. Jones, C.A. Mitchell, Preconditioned 70S30C bioactive glass foams promote osteogenesis in vivo, Acta Biomater. 9 (2013) 9169-9182.

[15] M. Catauro, F. Bollino, F. Papale, C. Ferrara, P. Mustarelli, Silica-polyethylene glycol hybrids synthesized by sol-gel: Biocompatibility improvement of titanium implants by coating, Materials Science and Engineering C 55 (2015) 118-125.

[16] T. Ozawa, A new method of analyzing thermogravimetric data, Bull. Chem. Soc. Jpn. 38 (1965) 1881-1886.

[17] J.H. Flynn, L.A. Wall, A quick, direct method for the determination of activation energy from thermogravimetric data, J. Polym. Sci., Part B: Polym. Lett. 4 (1966) 323-328.

[18] C.D. Doyle, Estimating isothermal life from thermogravimetric data, J. Appl. Polym. Sci. 6 (1962) 639-642.

[19] S. Vecchio Ciprioti, M. Catauro, Synthesis, structural and thermal behavior study of four Ca-containing silicate gel-glasses: Activation energies of their dehydration and dehydroxylation processes, J. Therm. Anal. Calorim. (In Press, 2015), DOI: 10.1007/s10973-015-4729-3.

[20] C. Duce, S. Vecchio Ciprioti, L. Ghezzi, V. Ierardi, M.R. Tine, Thermal behavior study of pristine and modified halloysite nanotubes - A modern kinetic study, J. Therm. Anal. Calorim. 121 (2015) 1011-1019.

[21] S. Vecchio, S. Materazzi, L.W. Wo, S. De Angelis Curtis, Thermoanalytical study of imidazole-substituted coordination compounds: Cu(II)- and Zn(II)-complexes of bis(1-methylimidazol-2-yl)ketone, Thermochim. Acta 568 (2013) 31-37.

[22] A. Zianna, S. Vecchio, M. Gdaniec, A. Czapik, A. Hatzidimitriou, M. Lalia-Kantouri, Synthesis, thermal analysis, and spectroscopic and structural characterizations of zinc(II) complexes with salicylaldehydes, J. Therm. Anal. Calorim. 112 (2013) 455-464.

[23] C. Papadopoulos, N. Kantiranis, S. Vecchio, M. Lalia-Kantouri, Lanthanide complexes of 3-methoxy-salicylaldehyde, J. Therm. Anal. Calorim. 99 (2010) 931-938.

[24] S. Vyazovkin, C.A. Wight, Kinetics in solids, Annu. Rev. Phys. Chem. 48 (1997) 125-149.

[25] P. Simon, Isoconversional methods - fundamentals, meaning and application, J. Therm. Anal. Calorim. 76 (2004) 123-132.

[26] J.R. Prado, S. Vyazovkin, Activation energies of water vaporization from the bulk and from laponite, montmorillonite, and chitosan powders, Thermochim. Acta, 524 (2011) 197-201.

[27] P. Saravanapavan, L.L. Hench, Mesoporous calcium silicate glasses. I. Synthesis, J. Non-Cryst. Solids 318 (2003) 1-13.

[28] A. Meiszterics, K. Sinkó, Sol–gel derived calcium silicate ceramics, Colloids and Surfaces A: Physicochemical and Engineering Aspects 319 (2008) 143-148.

[29] M. Catauro, F. Bollino, F. Papale, S. Vecchio Ciprioti, Investigation on bioactivity, biocompatibility, thermal behavior and antibacterial properties of calcium silicate glass coatings containing Ag, J. Non-Cryst. Solids 422 (2015) 16-22.

[30] D.E. Irish, G.E. Walrafen, Raman and infrared spectral studies of aqueous calcium nitrate solutions, J. Chem. Phys. 46 (1967) 378-384.

[31] B. Tiwari, A. Dixit, G.P. Kothiyal, M. Pandey, S.K. Deb, Preparation and characterization of phosphate glasses containing titanium, BARC Newsl., 285 (2007) 167-173.

[32] P. Innocenzi, Infrared spectroscopy of sol-gel derived silica-based films: a spectra-microstructure overview, J. Non-Cryst. Solids 316 (2003) 309-319.

[33] V. Simon, D. Eniu, A. Gritco, S. Simon, Thermal and spectroscopic investigation of sol-gel derived aluminosilicate bioglass matrices, J. Optoelectron. Adv. Mater. 9 (2007) 3368-3371.

[34] A. Buri, A. Costantini, G. Laudisio, R. Fresa, M. Catauro, F. Branda, Low temperature synthesis, structure and bioactivity of $xCaO\cdot(1\text{-}x)SiO_2$ glasses, J. Therm. Anal. 49 (1997) 863-868.

[35] A.M. Piccirillo, M. Ciarletta, S.D. Borysenko, Impulsive wendroff's type inequalities and their applications, AAPP Atti della Accademia Peloritana dei Pericolanti, Classe di Scienze Fisiche, Matematiche e Naturali, 90 (2012).

[36] V.F.F. Barbosa, K.J.D. MacKenzie, C. Thaumaturgo, Synthesis and characterisation of materials based on inorganic polymers of alumina and silica: sodium polysialate polymers, International J. Inorg. Mater. 2 (2000) 309-317.

[37] L. Radev, Influence of thermal treatment on the structure and in vitro bioactivity of sol-gel prepared $CaO\text{-}SiO_2\text{-}P_2O_5$ glass-ceramics, Processing and Application of Ceramics 8 (2014) 155-166.

[38] A.M. Piccirillo, S.S. Borysenko, S.D. Borysenko, Qualitative analysis behaviour of the solutions of impulsive differential systems, AAPP Atti della Accademia Peloritana dei Pericolanti, Classe di Scienze Fisiche, Matematiche e Naturali, 89 (2011).

Captions to figures

Fig. 1 Images of representative obtained samples: A) 63S32C5P and B) 61S38C1P wet gels

Fig. 2 Flow chart of the synthesis process.

Fig. 3 Simultaneous TG/DTA curves (plots a and b, respectively) of the gel glasses investigated in Ar flowing atmosphere (50 ml min^{-1}) at 10 K min^{-1}.

Fig. 4 Conversion dependency of activation energy of dehydration, determined by the OFW method. Estimated uncertainties are always less than 8 kJ mol^{-1}.

Fig. 5 FTIR spectra of: A) Synthesized $SiO_2 \cdot CaO \cdot P_2O_5$ samples and B) pure $Ca(NO_3)_2 \cdot 4H_2O$ and control materials.

Fig. 6 Enlarged view of the FTIR spectra of the four gel glasses in the region between 1300 and 800 cm^{-1}.

Fig. 7 FTIR spectra of the synthesized $SiO_2 \cdot CaO \cdot P_2O_5$ samples compared with pure SiO_2 spectrum after heat treatment at 600°C.

Fig. 8 FTIR spectra of the synthesized $SiO_2 \cdot CaO \cdot P_2O_5$ samples after heat treatment at 1200°C.

Fig. 9 SEM image of: A) 63S32C5P and B) 61S38C1P after 120°C and EDX spectra of the surface; C) 63S32C5P and D) 61S38C1P after 600°C; E) 63S32C5P and F) 61S38C1P after 1200°C and EDX of crystal in the ring.

Fig. 10 X-ray diffraction pattern of fresh (only 61S38C1P and 63S32C5P) and calcined (at 1200°C) samples (plots a and b, respectively). Pseudowollastonite (*), wollastonite ($^{+}$) and $Ca_{15}(PO_4)_2(SiO_4)_6$ ($^{\#}$).

392

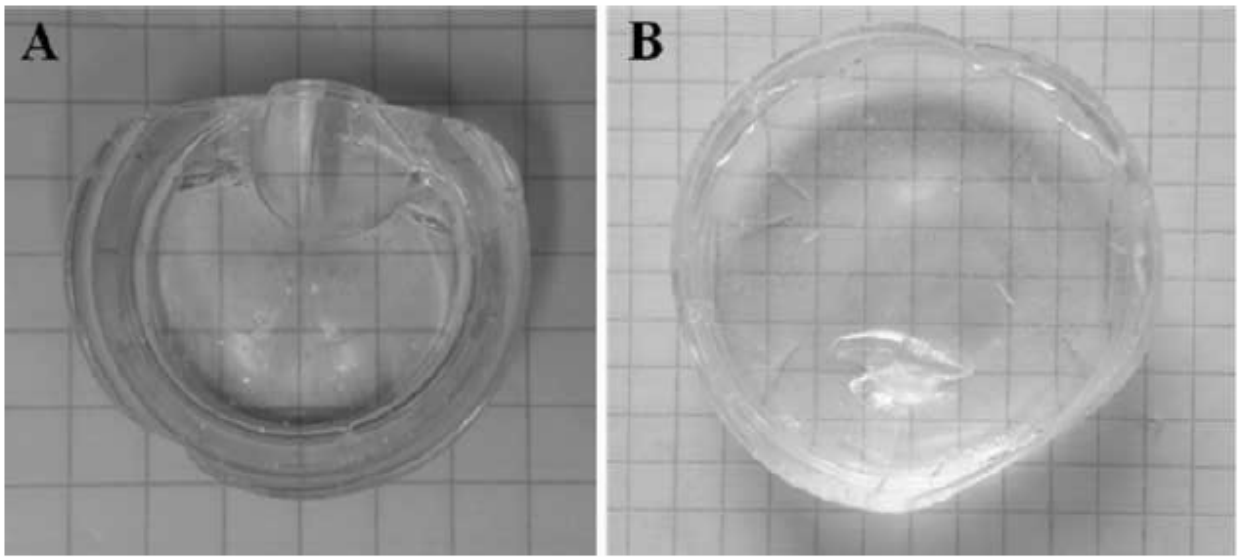

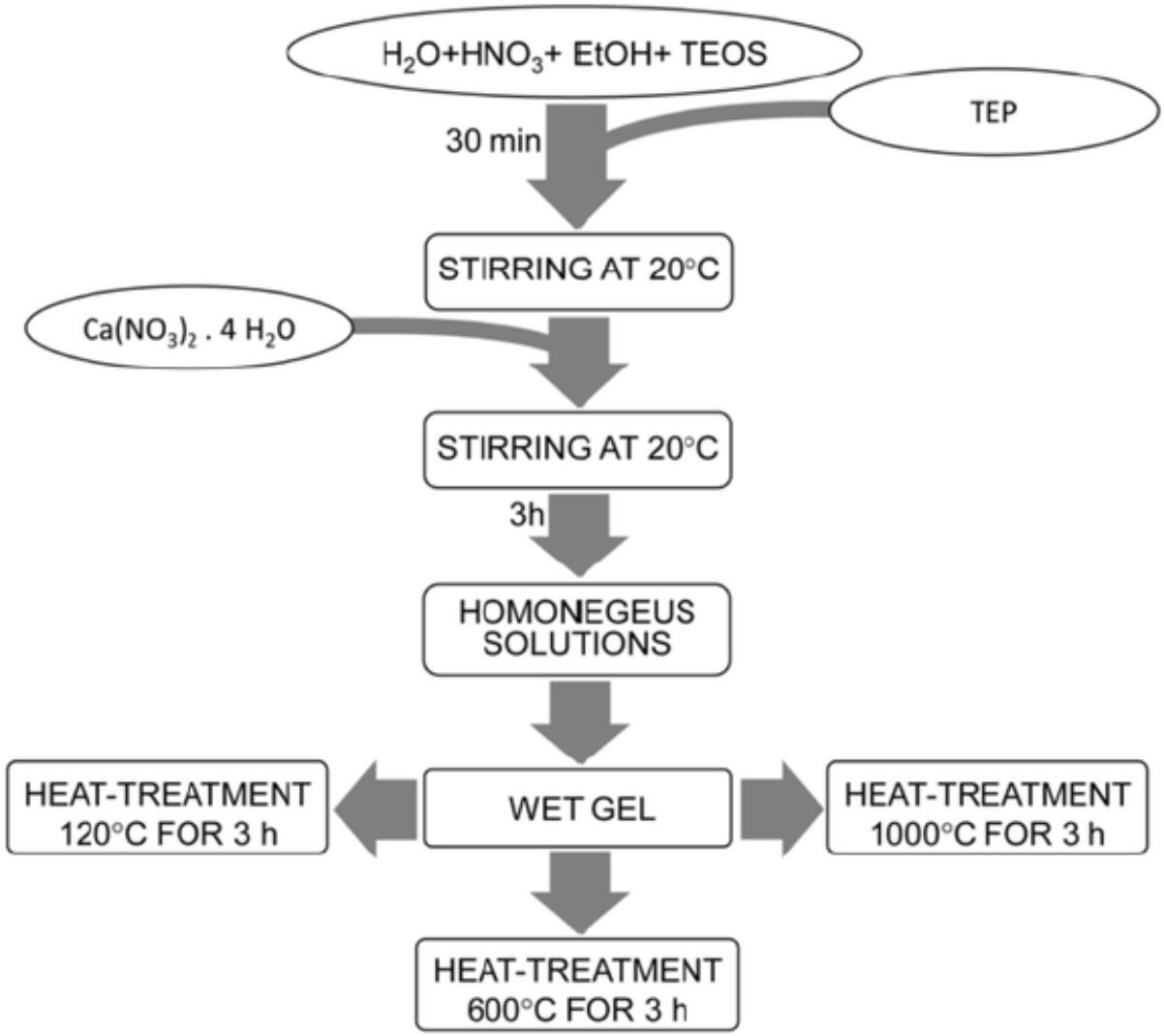
H_2O+HNO_3+ EtOH+ TEOS
TEP
30 min
STIRRING AT 20°C
$Ca(NO_3)_2$. 4 H_2O
STIRRING AT 20°C
3h
HOMONEGEUS SOLUTIONS
HEAT-TREATMENT 120°C FOR 3 h
WET GEL
HEAT-TREATMENT 1000°C FOR 3 h
HEAT-TREATMENT 600°C FOR 3 h

393
394

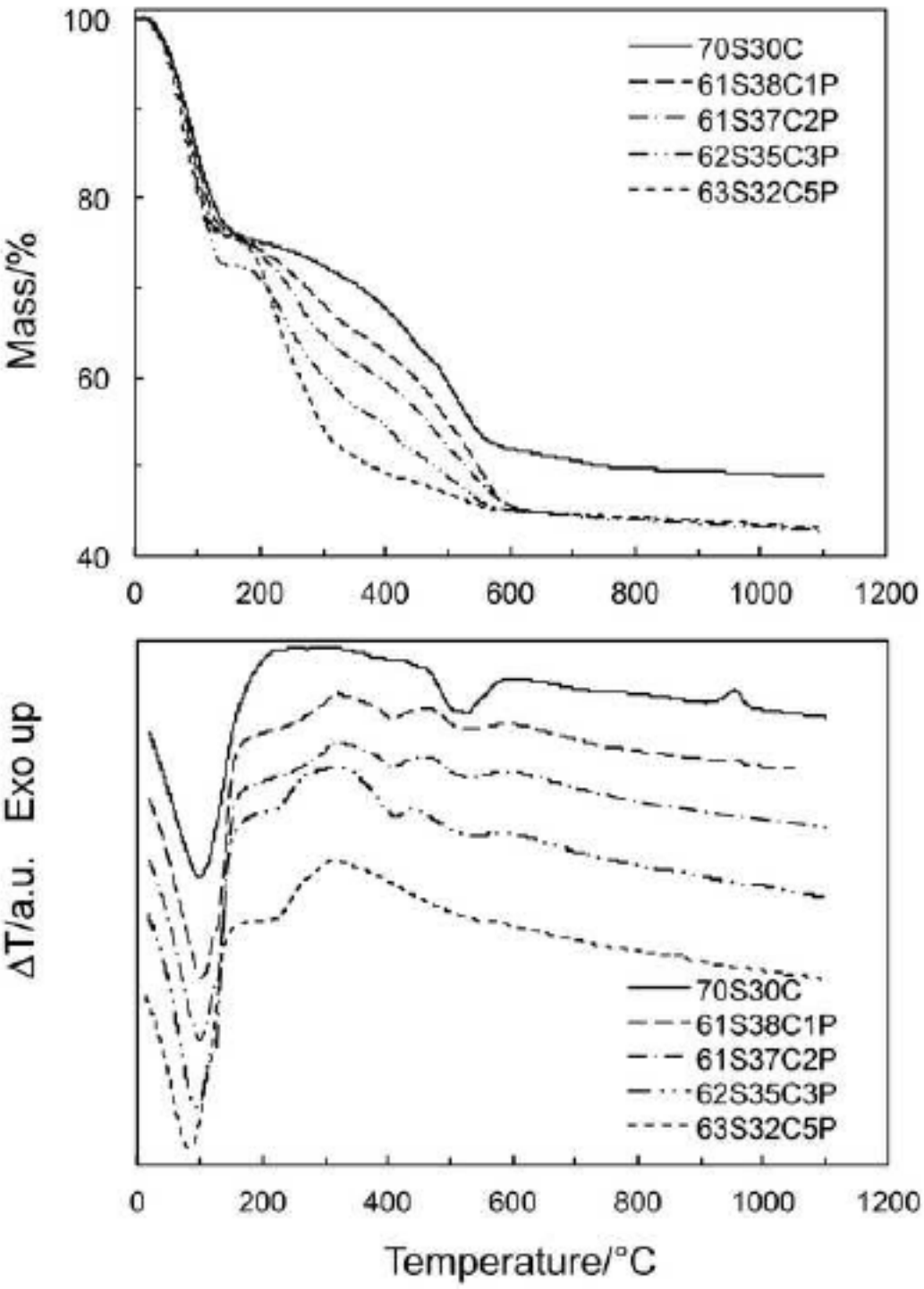
100
80
60
40
Mass/%
0
200
400
600
800
1000
1200
70S30C
61S38C1P
61S37C2P
62S35C3P
63S32C5P
ΔT/a.u. Exo up
Temperature/°C

395

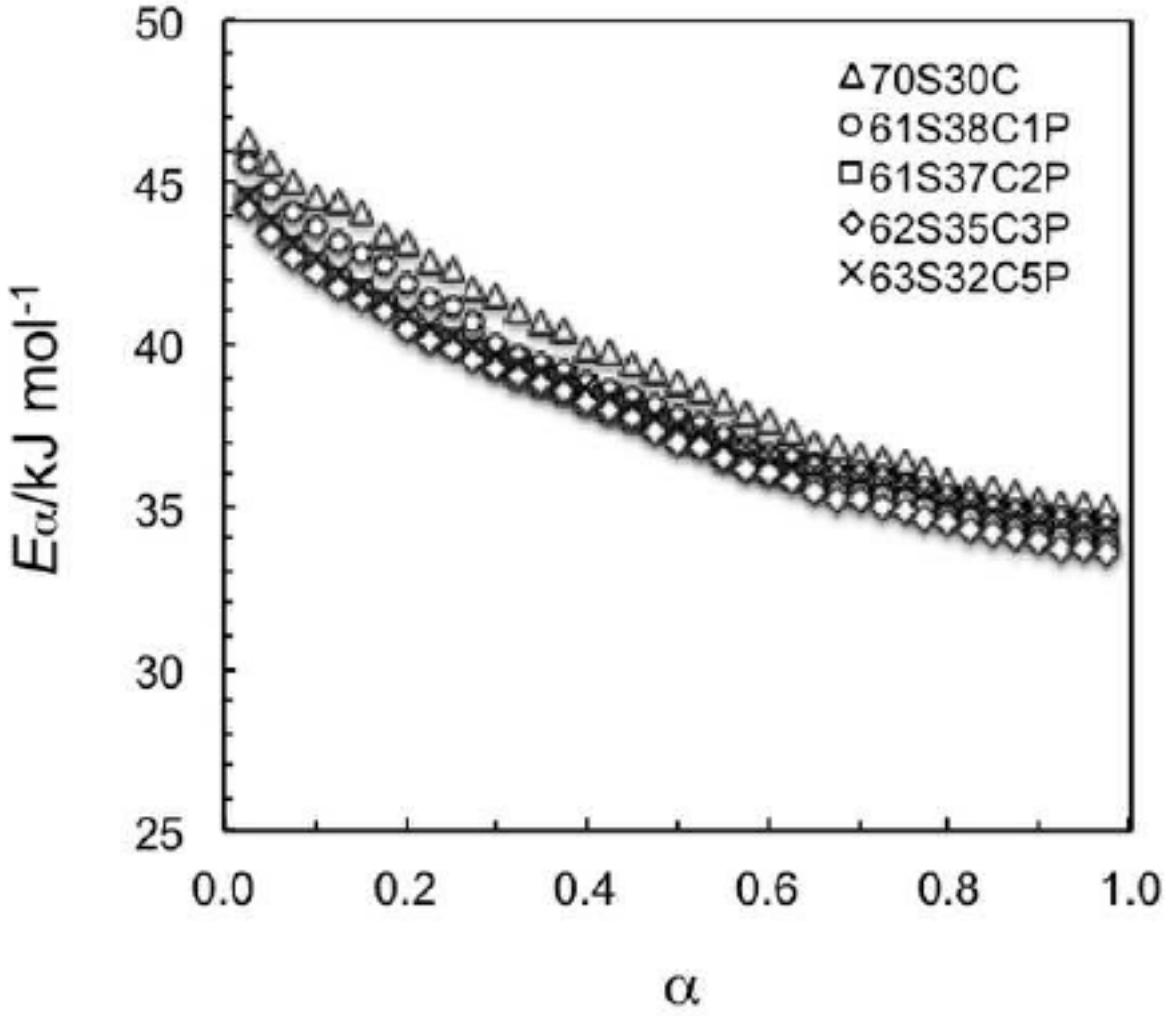
50
45
40
35
30
25
0.0
0.2
0.4
0.6
0.8
1.0
α
Eα/kJ mol-1
△70S30C
○61S38C1P
□61S37C2P
◇62S35C3P
×63S32C5P

396

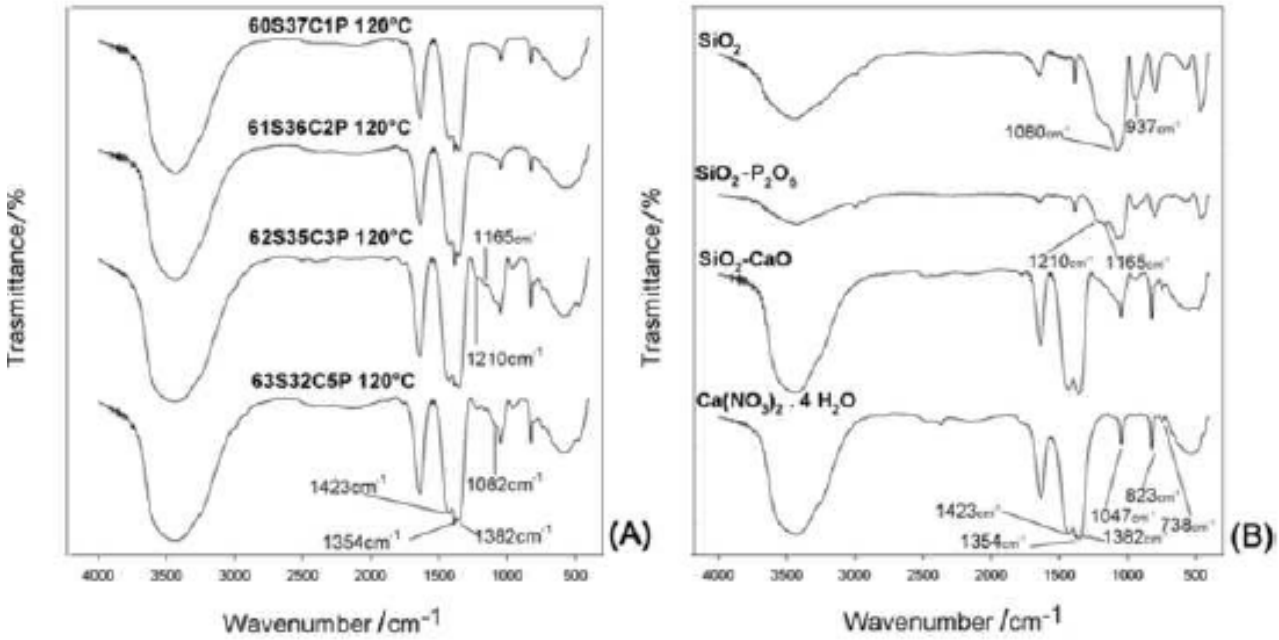
60S37C1P 120°C
61S36C2P 120°C
62S35C3P 120°C
63S32C5P 120°C
1165cm-1
1210cm-1
1423cm-1
1082cm-1
1354cm-1
1382cm-1
(A)
Trasmittance/%
Wavenumber /cm-1
SiO2
1080cm-1
937cm-1
SiO2-P2O5
SiO2-CaO
1210cm-1
1165cm-1
Ca(NO3)2 . 4 H2O
823cm-1
1423cm-1
1047cm-1
738cm-1
1354cm-1
1382cm-1
(B)
Trasmittance/%
Wavenumber /cm-1

397

398

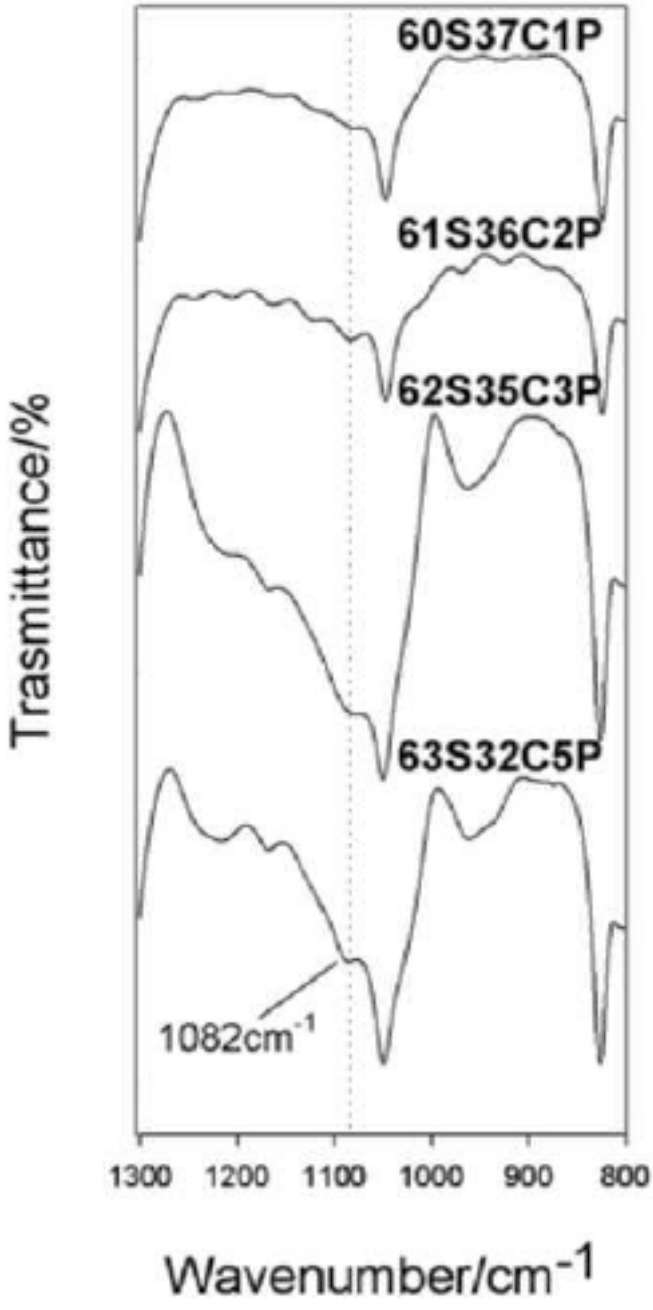
60S37C1P
61S36C2P
62S35C3P
63S32C5P
1082cm-1
Trasmittance/%
1300
1200
1100
1000
900
800
Wavenumber/cm-1

399

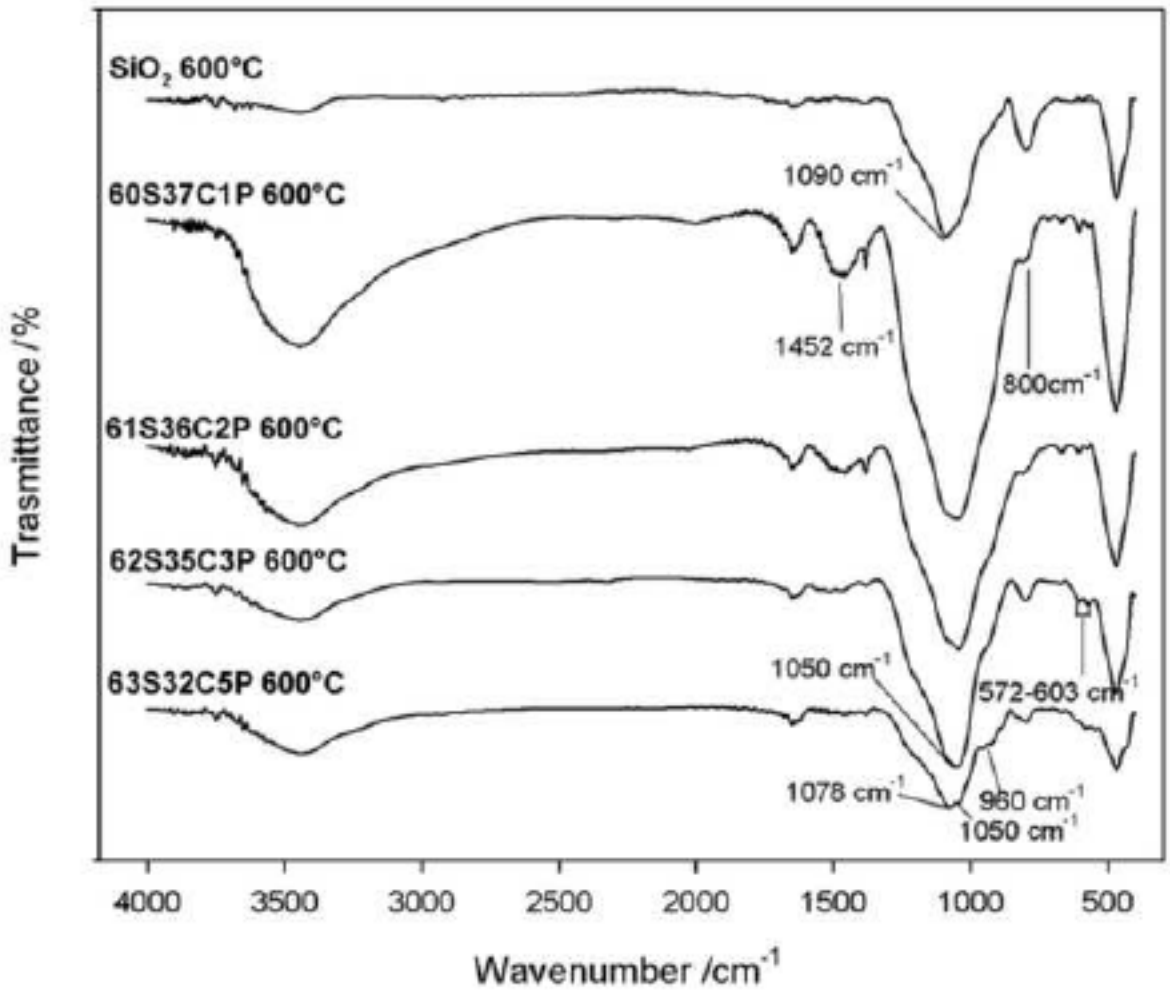
SiO2 600°C
60S37C1P 600°C
61S36C2P 600°C
62S35C3P 600°C
63S32C5P 600°C
1090 cm-1
1452 cm-1
800cm-1
1050 cm-1
572-603 cm-1
1078 cm-1
960 cm-1
1050 cm-1
Trasmittance /%
4000
3500
3000
2500
2000
1500
1000
500
Wavenumber /cm-1

400

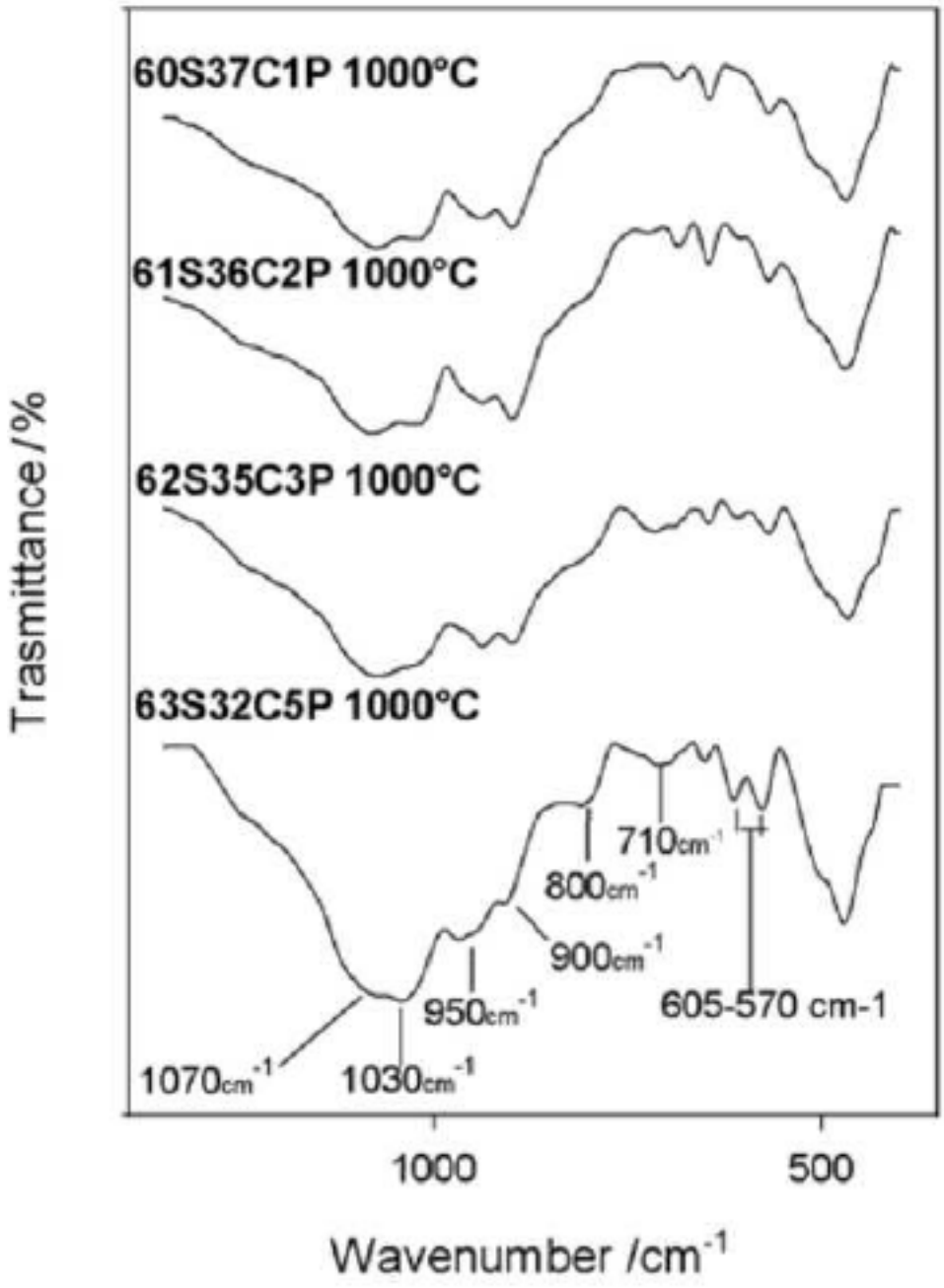
60S37C1P 1000°C
61S36C2P 1000°C
62S35C3P 1000°C
63S32C5P 1000°C
Trasmittance /%
710cm-1
800cm-1
900cm-1
950cm-1
605-570 cm-1
1070cm-1
1030cm-1
1000
500
Wavenumber /cm-1

401

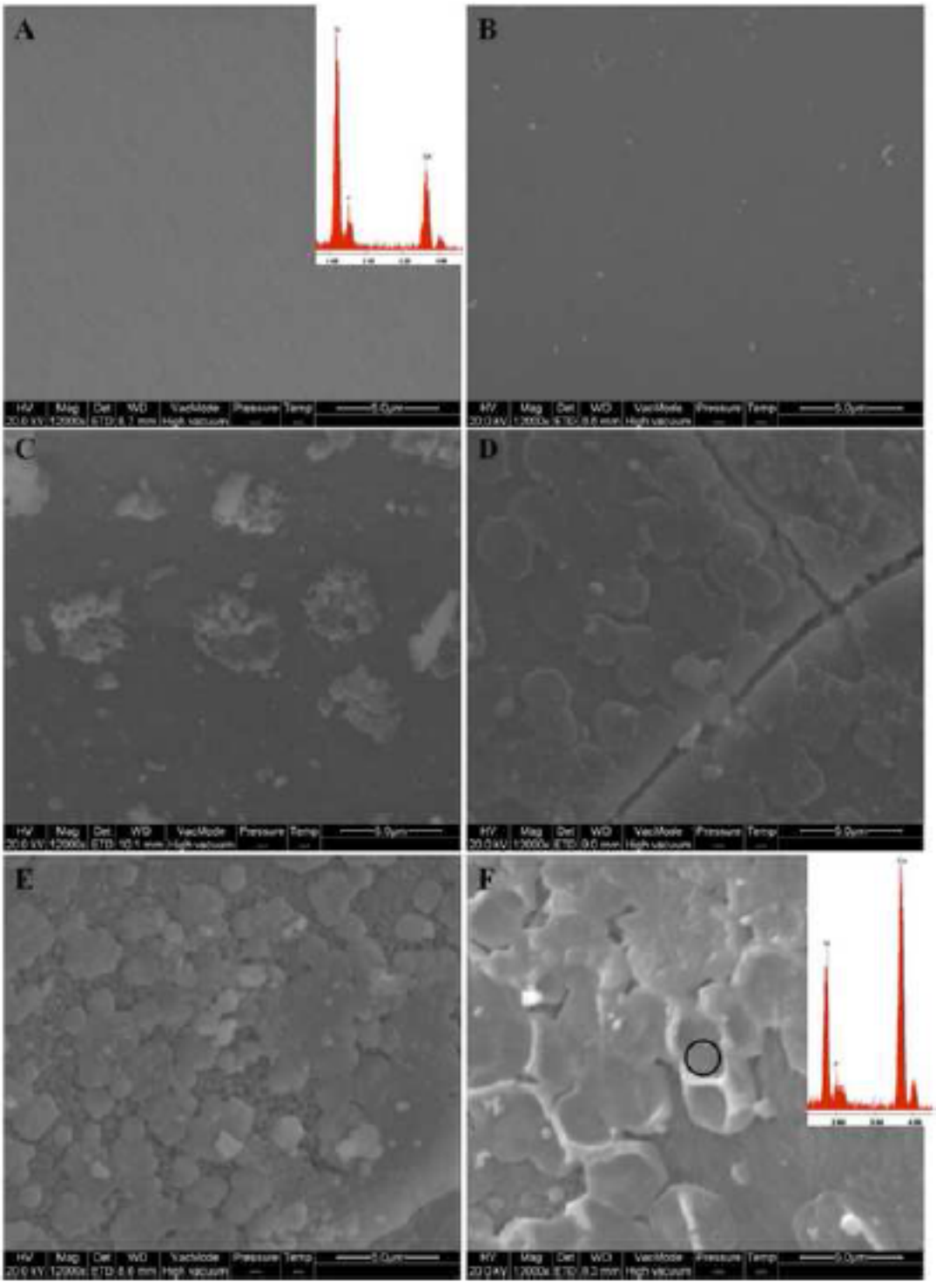

402

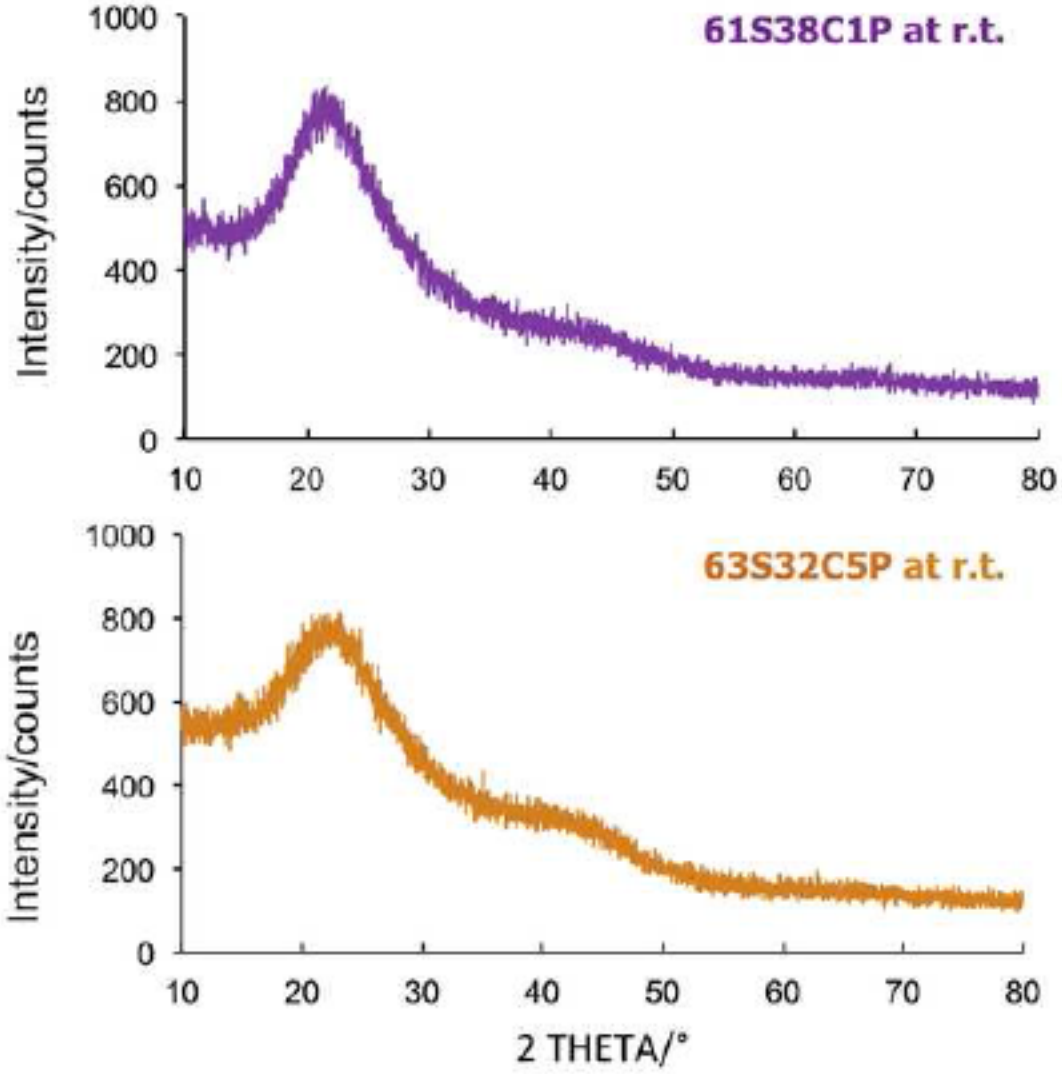
61S38C1P at r.t.
Intensity/counts
1000
800
600
400
200
0
10
20
30
40
50
60
70
80
63S32C5P at r.t.
Intensity/counts
1000
800
600
400
200
0
10
20
30
40
50
60
70
80
2 THETA/°

403

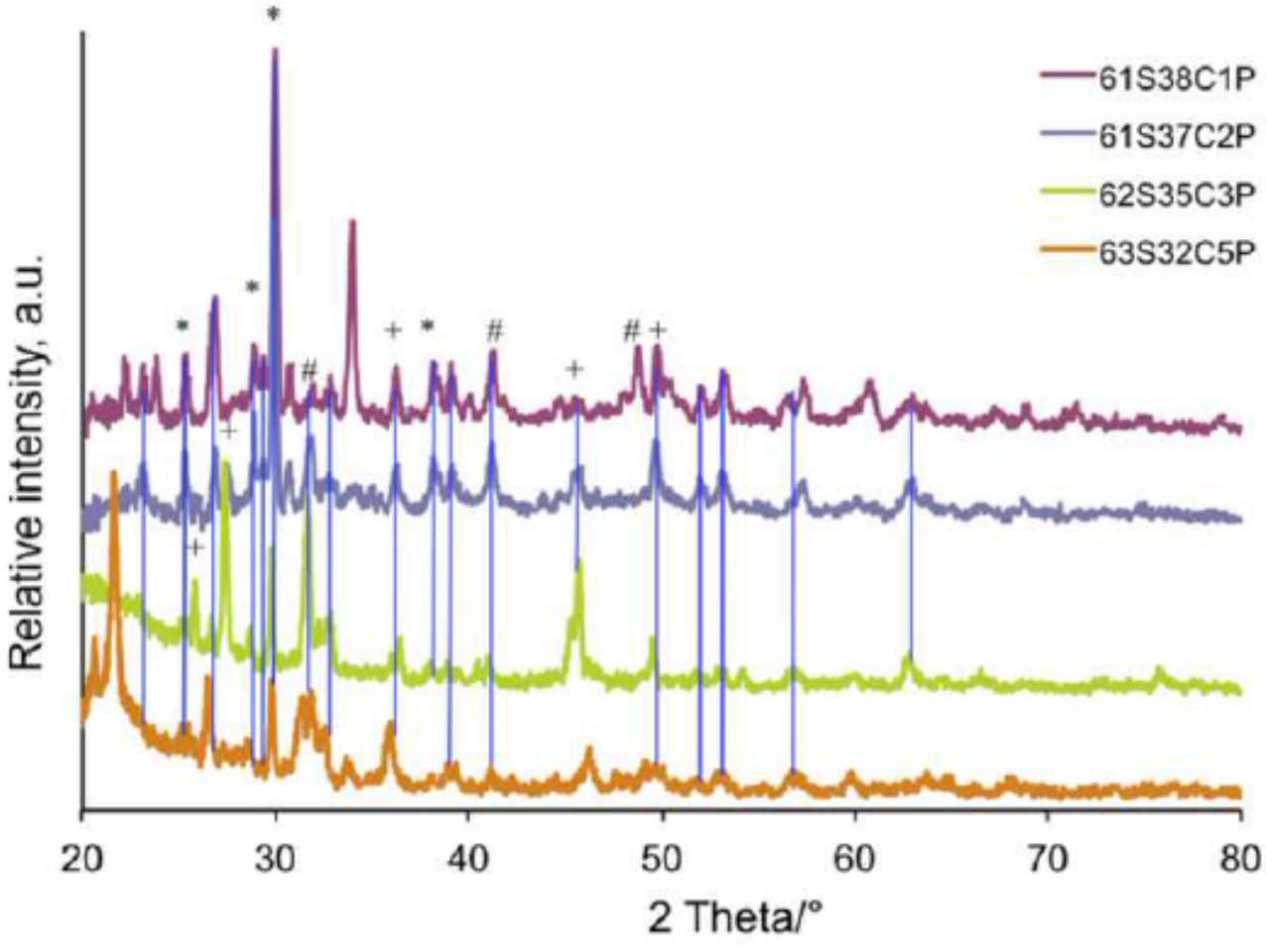
61S38C1P
61S37C2P
62S35C3P
63S32C5P
Relative intensity, a.u.
2 Theta/°
20
30
40
50
60
70
80